Microstructures and electrochemical properties of Si-Ni based alloys fabricated by melt spinning process

J.J.Song, K.S.Kim, H.J.Kim, H.J.Kwon, S.K.Nam, K.Y.Sohn, W.W.Park

Department of Nano System Engineering, Inje University, 607 obang-dong, Gimhae, Gyeongnam 621-749, Republic of Korea

Corresponding author: [Tel: +82-55-326-9501, E-mail: wwpark@inje.ac.kr]

ABSTRACT

In this work, Si-Ni-Al and Si-Ni-Cu-Al alloy ribbons were fabricated by melt spinning process to minimize the effect of the volume change of silicon particles. $Si_{52}Ni_{41}Al_7$ and $Si_{50}Ni_{25}Cu_{15}Al_{10}$ alloy ribbons by atomic ratio were prepared by arc-melting followed by melt spinning process. The melt-spun ribbons were fragmented to produce powder. Subsequently, acetylene black (AB), polyvinylidene fluoride (PVDF) and N-methylpyrrolidinone (NMP, 7cc) were added into the alloy powder and mixed by planetary milling for 2 hours. The electrochemical properties of the cells were measured at 100 mAh/g current density between 0.01 and 2.0V. Microstructural evaluation and phase analysis were conducted by transmission electron microscopy (TEM) and scanning electron microscopy (SEM) combined with energy-dispersive spectrometry (EDS).

Keywords: melt-spun ribbons, microstructures, electrochemical properties

1 INTRODUCTION

Lithium ion battery(LIB) is one of the most significant high energy power sources. Graphite has been used extensively as the commercial anode material for the batteries due to its excellent cycling behavior upon repeated charge and discharge cycles [1]. In general, graphite or other carbonaceous materials are state-of-the-art in lithium ion batteries as active mass in negative electrodes. However, the theoretical capacity of graphite is limited to 372 mAh/g [2, 3]. Therefore studies for developing high performance anode materials have been conducted to overcome the limitations in the capacity of lithium-ion batteries and achieve improvements in terms of cycle life, safety and to enlarge the temperature operation field. Silicon-based anode materials have been studied as a replacement of graphite or carbon anode materials because of its high theoretical capacity (4,200 mAh/g) [4], whereas Si shows a drastic volume expansion/contraction during Li^+ insertion/ extraction. This causes the pulverization of Si particles and loose contacts between Si particles and current collector resulting in the mechanical instability and poor cycle ability. The volume change and adherence to current collector of Si active material have been regarded as the key factors to the electrochemical stability of Si anodes [5, 6]. Si powders with small particle size could decrease the volume expansion during cycling [7]. Another approach is the electrochemically inactive with lithium phase acts as a buffer to suppress of accommodate the large volume changes of the active host materials [5]. In our experiments, Si-Ni-Al and Si-Ni-Cu-Al alloy ribbons were fabricated by a rapid solidification process at the cooling rate of about one million ℃/sec to minimize the effect of the volume change of silicon particles. These have compared in accordance with addition of materials and have shown promising results following the good microstructure. In addition, the electrochemical properties of the cells were measured by C-V test and cycle test.

2 EXPERIMENTAL PROCEDURE

The Si based anode material were prepared using 99.999% pure silicon, 99.99% pure nickel, 99.999% pure aluminum and 99.999% pure cupper. Ingots (Table 1) with a mass of approximately 10g were produced by arc melting in an arc melting in an arc furnace with a water-cooled copper hearth under an inert atmosphere by injecting high-purity argon. Directionally grown samples were produced utilizing a vertical Bridgman type device with induction heating and Graphite Nozzle and tubes, which served as crucibles. Ingots 5.0 cm long and 0.7 cm in diameter were prepared by moving the crucibles with the metallic samples from the upper hot region to the lower cold region under an argon atmosphere. The solidification rate ranged from 10.0 to 180.0 mm/h at a thermal gradient of around 100 ◦C/cm at the solid/liquid interface. The temperature of the hot region was set at 1300 ◦C and was controlled with an optical pyrometer. Rapidly quenched ribbon was processed using a copper wheel at a tangential velocity of approximately 32 m/s and melt ejected at 1300 ◦C with an overpressure of 1.25mgf/cm^2. After processing by optimizing melt spinning, the solidified samples were cut into transverse and longitudinal sections and prepared by grinding, mechanical polishing and chemical etching for further metallographic analysis. The analysis included an examination of the growth morphology resulting from the solidification conditions, using optical and scanning electron microscopy. In addition, an X-ray diffraction analysis using the Cu K- line was carried out in order to evaluate metastable phase formation.

	Si	Ni	Al
wt%	52	41	7

(a)

	Si	Ni	Cu	Al
wt%	50	25	15	10

(b)

Table 1. Chemical compositions of (a) Si-Ni-Al, (b) Si-Ni-Cu-Al alloys

3 RESULT & DISCUSSION

3. 1 XRD characterization of the materials

The X-ray diffraction patterns of the Si_{52}-Ni_{41}-Al_7 and Si_{50}-Ni_{25}-Cu_{15}-Al_{10} alloy strips are shown in Fig.1. The diffraction lines of Fig 1(a) are only indexed to Si and NiSi2 and the diffraction lines of Fig 1(b) are attributed to electrochemically inactive materials (Si-Ni alloys, intermetallic compound). The data suggests that a distinct Si peak of Si_{52}-Ni_{41}-Al_7 appears in the products at 28.4°, but no pure diffraction peak of Si_{50}-Ni_{25}-Cu_{15}-Al_{10} is observed. When the reactant proportion is changed and Cu is added to ingot of Si-Ni-Al, the intensity of Si peak decreased but still is observed. It is expected that new phases such as SiC would form during the melt spinning process because graphite nozzles were used as a crucible. But, no new diffraction peaks were observed during XRD analysis. The intensity of the Si peak increases in accordance with increase in the Si content and Si is identified as a crystalline phase.

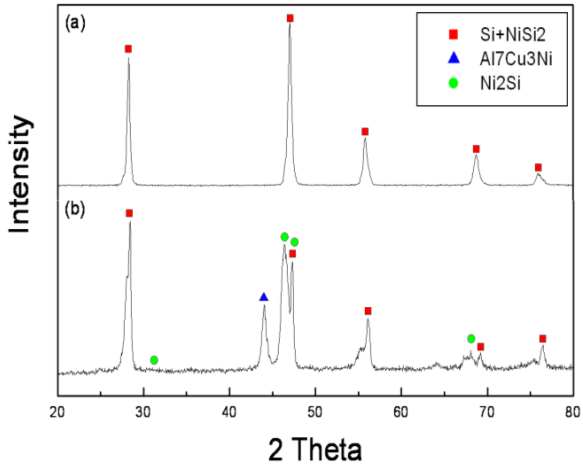

Figure 1: X-ray diffraction patterns: (a) Si_{52}-Ni_{41}-Al_7 (b) Si_{50}-Ni_{25}-Cu_{15}-Al_{10} alloy thin strips

3.2 SEM characterization

The SEM images of cross-sections of Si_{52}-Ni_{41}-Al_7 alloy thin strip are shown by second electrons (SE) in Fig 2 and Si_{50}-Ni_{25}-Cu_{15}-Al_{10} alloy thin strip are shown by backscattered electrons (BSE) in Fig 3. These indicate that several of Si particles are surrounded by inactive matrix such as Si-Ni alloy phases which acts as a buffer to suppress the volume change. Fig 2(c) shows that most of the Si particle shapes are fine, coarse, dendrite and spiculate and the estimated average size of the Si particles of Si_{52}-Ni_{41}-Al_7 alloy thin strip is approximately 20nm ~ 200nm in diameter and Si particles of Si_{50}-Ni_{25}-Cu_{15}-Al_{10} alloy thin strip in Fig 3 also has the same shapes with the diameter of about 100nm ~ 300nm. In the SEM images of cross-sections of Fig 2(a) shown the air-side, Si particles are more coarsened because cooling rate is not rapid enough to produce Si-Ni base alloy strips. On the other hand, Fig 2(b) seen the wheel-side Si particles are become more and more fine particle such as nano scale.

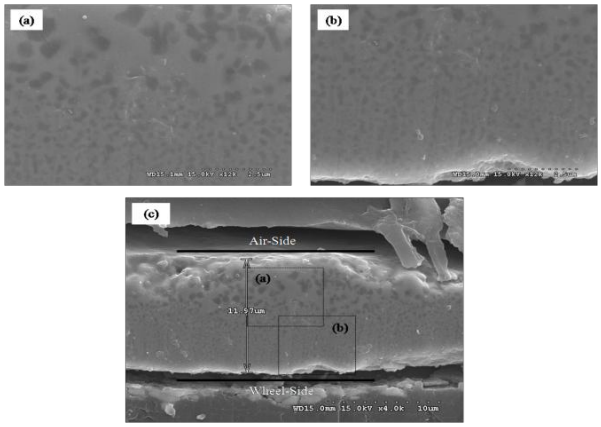

Figure 2: The SEM images: (a) air-side (b) wheel-side (c) Si_{52}-Ni_{41}-Al_7 alloy thin strip

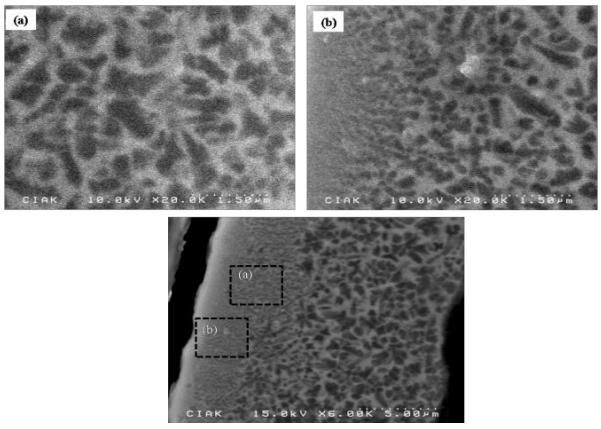

Figure 3: The SEM images: (a) middle-side (b) wheel-side (C) Si_{50}-Ni_{25}-Cu_{15}-Al_{10} alloy thin strip

Fig 3(c) shows that Si particle phases of Si_{50}-Ni_{25}-Cu_{15}-Al_{10} alloy thin strip have similar with Si_{52}-Ni_{41}-Al_7 alloy thin strip but, coarse particles of Si are more widely distributed than Si particles of Si_{52}-Ni_{41}-Al_7 alloy thin strip. In addition, the Si-Ni base alloy is composed electrochemically active Si phase and inactive phases that were identified using EDS analysis. The dark region indicates Si and the grey region indicates intermetallic compound ($NiSi_2$, Ni_2Si and etc). The amount of inactive phase synthesized during the melt spinning process in accordance with the composition of the starting materials. The Si-Ni base alloy is suitable to suppress the large volume change of Si during cycling. Hence, it is expected that the electrochemically inactive phases provide structural integrity to the active material and thereby provide stability to the system and capacity retention.

3.3 TEM characterization

TEM is a more effective method to observe the microstructure of Si_{52}-Ni_{41}-Al_7 and Si_{50}-Ni_{25}-Cu_{15}- Al_{10} alloy thin strips. Fig 4 and 5 Show the TEM mapping images of Si_{52}-Ni_{41}-Al_7 and Si_{50}-Ni_{25}-Cu_{15}-Al_{10} alloy thin strips. At TEM mapping images, bright areas are Si particles and dark areas are Si-Ni compounds. Fig 6 and 7 are TEM images and corresponding SAED patterns of Si_{52}-Ni_{41}-Al_7 and Si_{50}-Ni_{25}-Cu_{15}-Al_{10} alloy thin strips. The dispersed and very ambiguous selected area electron diffraction (SAED) pattern in the inset of Fig 6 and 7 prove that the Si particle is polycrystalline.

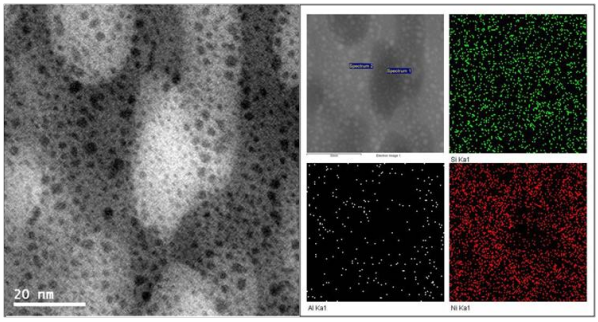

Figure 4: TEM mapping image of Si-Ni-Al alloy ribbon

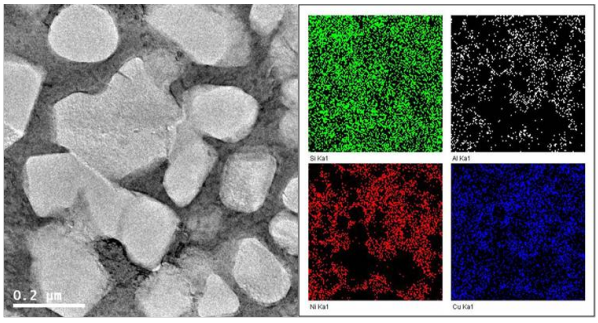

Figure 5: TEM mapping image of Si-Ni-Cu-Al alloy ribbon

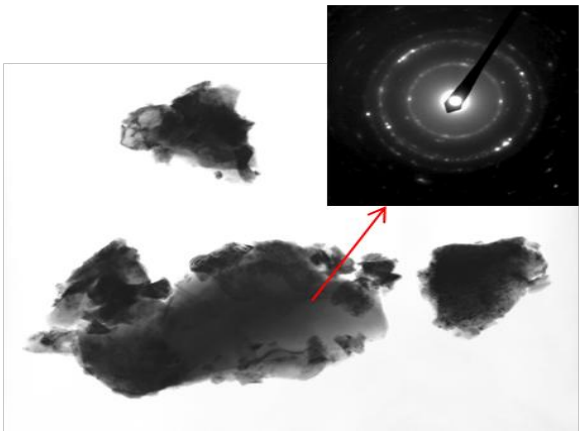

Figure 6: TEM image and corresponding SAED patterns of Si particle of Si-Ni-Al alloy powder

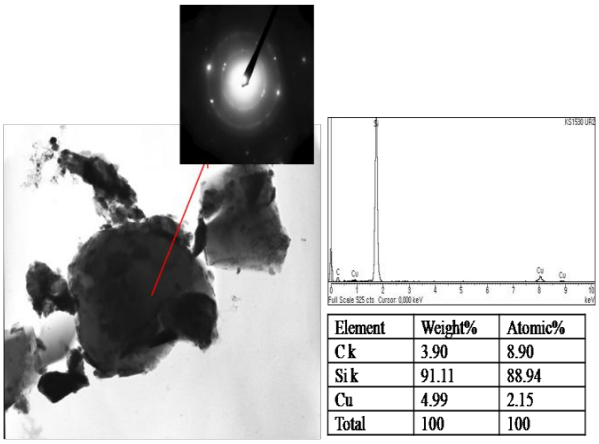

Element	Weight%	Atomic%
C k	3.90	8.90
Si k	91.11	88.94
Cu	4.99	2.15
Total	100	100

Figure 7: TEM image and corresponding SAED patterns of Si particle of Si-Ni-Cu-Al alloy powder

4 CONCLUSION

In order to improve the characteristics of anode material for Li-ion battery, Si-Ni base thin strips were rapidly solidified by melt spinning. It is reported that the amorphous structure of Si anode material is beneficial to the electrochemical performance because amorphous material shows homogeneous volume expansion/contraction during Li+ insertion/extraction and has many Li+ diffusion paths [8].

1. In $Si_{52}Ni_{41}Al_7$ alloy ribbons, the primary Si particles of 20~200nm size were dispersed in the $NiSi_2$ matrix. Relatively coarse particles were formed because a cooling rate of melt spinning was not enough to form small Si particles (<50nm).

2. In Si_{50}-Ni_{25}-Cu_{15}-Al_{10} ribbons, the primary Si particles of

100~300nm size were also dispersed in the $SiNi_2$, Al_7Cu_3Ni, $NiSi_2$ matrix.

3. Inactive matrixes ($NiSi_2$ $SiNi_2$, Al_7Cu_3Ni), which have good mechanical properties, were formed in ribbons.

4.To disperse small Si particles regulary in amorphous matrix, a cooling rate of melt spinning should be increased.

REFERENCES

[1] Min-Sik Park, S. Rajendran, uong-mook kang, kyu-Sung han, Young-Soo han, Jai-Young Lee, J. Power Sources 158, 650-653, 2006

[2] R. Yazami, k. Zaghib, M. Deschamps, J. Power Sources 52 ,55-59, 1994

[3] J. Yang, Y. Takeda, N. Imanish, O, Yamamoto, J. Electrochem. Soc. 146, 4009-4013, 1999

[4] Li H, Huang X, Chen L et al // Electrochem Solid-State Lett 2, 547, 1999

[5] Chen L, Xie X, Wang B et al // Mat Sci Eng B 131, 186, 2006

[6] Chen L, Xie X, Xie J et al // J Appl Electrochem. 36, 1099, 2006

[7] I.S. kim, P. Kumta, G.E. Blomgren, Electrochem. Solid State let. 3, 493-496, 2000

[8] A. Netz, R.A. Huggins, W. Weppner, // J. power Sources 95, 119, 2003